Sensors and Materials, Vol. 36, No. 6 (2024) 2643–2654
MYU Tokyo

S & M 3692

Speed Prediction Direct-torque-controlled Induction Motor Drive Based on Motor Resistance Parameter Identification

Yung-Chang Luo,* Jian-Chien Tsai, Hao-You Huang, and Wen-Cheng Pu

Department of Electrical Engineering, National Chin-Yi University of Technology,
No. 57, Sec. 2, Zhongshan Rd, Taiping Dist, Taichung 41170, Taiwan (ROC)

(Received December 21, 2023; accepted June 7, 2024)

Keywords: direct torque control (DTC), speed prediction, stator resistance parameter identification, model reference adaptive system (MRAS), modified particle swarm optimization (PSO) algorithm

A motor resistance parameter identification scheme was proposed for the speed prediction of a direct-torque-controlled (DTC) induction motor (IM) drive. The DTC IM drive was established on the basis of the stator's current and flux, with the stator current acquired from an IM using the Hall effect current sensor. Rotor speed prediction was achieved using the electromagnetic torque and rotor flux. The stator resistance parameter identification scheme was developed using the model reference adaptive system based on the motor's active power, and the adaptation mechanism was designed using the modified particle swarm optimization algorithm. The MATLAB\Simulink® toolbox was utilized to simulate this system, and all the control algorithms were realized using a TI DSP 6713 and F2812 micro-control card to validate this approach. Simulation and experimental results confirmed the effectiveness of the proposed approach.

1. Introduction

The development of Industry 4.0 and electric vehicles necessitates high-performance actuators. Induction motors (IMs), compared with DC motors, are advantageous owing to their lack of commutators and carbon brushes, making them more suitable for high-power applications. AC motor direct torque control (DTC) lacks decoupling calculation and does not require coordinate transformation between synchronous and stationary reference frames. Compared with the field-oriented control, DTC is more suitable for motor drives that require rapid responses. The traditional DTC scheme is a switching table (ST) power switching pattern, and the current and torque ripples are notable. In place of the ST pattern by a voltage space vector pulse width modulation (VSVPWM) power switching pattern, the torque and current ripples can be reduced.[1] For the implementation of conventional closed-loop DTC IM drives, a shaft position sensor such as an encoder or a resolver is required to detect rotor position. However, this sensor deteriorates the drive robustness and is not suitable for hostile environments. Several speed estimation methods for DTC IM drives have been published: speed acquisition from a flux estimator,[2–4] speed estimation using an observer,[5–7] and speed

*Corresponding author: e-mail: luoyc@ncut.edu.tw
https://doi.org/10.18494/SAM4838

ISSN 0914-4935
https://myukk.org/

determination from an extended Kalman filter.[8–10] Furthermore, for the implementation of a speed prediction DTC IM drive, the parameters of stator and rotor resistances are required to estimate the stator flux, torque, and rotor speed. These parameters deviate from their actual values owing to temperature variations, resulting in drive performance degradation. Several motor resistance parameter identification approaches for IM drives have been presented in the literature: resistance parameter estimation according to a neural network,[11–13] resistance parameter determination by adopting adaptive control theory,[14–16] and resistance parameter identification using fuzzy logic control.[17–19] In this research, a DTC IM drive was established using the current and flux of the stator, and the detected three-phase stator currents were acquired from an IM through electromagnetic Hall effect current sensors. The predicted rotor speed was obtained on the basis of electromagnetic torque and rotor flux. A stator resistance parameter identification scheme was developed using a motor's active power according to the model reference adaptive system (MRAS), and the adaptation mechanism was designed using the modified particle swarm optimization (PSO) algorithm. These approaches confirmed the feasibility of implementing a promising speed prediction DTC IM drive using motor resistance parameter identification.

This paper comprises six sections. In Sect. 1, we present the research background and motivation, and review the literature on speed prediction methods for DTC IM drives using the motor resistance parameter identification. In Sect. 2, the DTC IM drive system and speed prediction method are described. The design details of the stator resistance parameter identification scheme based on MRAS are given in Sect. 3. In Sect. 4, we explain in detail the adaptation mechanism design using the modified PSO algorithm. Sections 5 and 6 cover the simulation and experimental results, discussion, and conclusions.

2. Speed Prediction DTC IM Drive with VSVPWM

The stator and rotor voltage equations of an IM in the stationary reference coordinate frame are given by[20]

$$R_s\vec{i}_s^{\,s} + p\vec{\lambda}_s^{\,s} = \vec{v}_s^{\,s}, \tag{1}$$

$$R_r\vec{i}_r^{\,s} + p\vec{\lambda}_r^{\,s} - j\omega_r\vec{\lambda}_r^{\,s} = 0, \tag{2}$$

where $\vec{i}_s^{\,s} = i_{ds}^s + ji_{qs}^s$ and $\vec{i}_r^{\,s} = i_{dr}^s + ji_{qr}^s$ are the stator and rotor currents, $\vec{\lambda}_s^{\,s} = \lambda_{ds}^s + j\lambda_{qs}^s$ and $\vec{\lambda}_r^{\,s} = \lambda_{dr}^s + j\lambda_{qr}^s$ are the stator and rotor fluxes, R_s and R_r are the stator and rotor resistances, respectively, $\vec{v}_s^{\,s} = v_{ds}^s + jv_{qs}^s$ is the stator voltage, ω_r is the electric speed of the rotor, $p = d/dt$ is the differential operator, and j stands for the imaginary part.

Under a DTC condition, the d-axis and q-axis estimated stator flux can be expressed as

$$\hat{\lambda}_{ds}^s = \frac{\kappa_c}{1+s\kappa_c}(v_{ds}^s - R_s i_{ds}^s) + \frac{1}{1+s\kappa_c}\lambda_{ds}^{s^*}, \tag{3}$$

$$\hat{\lambda}_{qs}^{s} = \frac{\kappa_c}{1+s\kappa_c}(v_{qs}^{s} - R_s i_{qs}^{s}) + \frac{1}{1+s\kappa_c}\lambda_{qs}^{s^*}, \tag{4}$$

where the symbol ^ denotes the estimated value, κ_c is the time constant of the low-pass filter, s is the Laplace operator, and λ_{ds}^{s} and $\lambda_{qs}^{s^*}$ are the d-axis and q-axis components of the stator flux reference, respectively.

On the basis of Eqs. (3) and (4), the estimated synchronous position angle for implementing the DTC IM drive is given by

$$\hat{\theta}_e = \tan^{-1}\left(\frac{\hat{\lambda}_{qs}^{s}}{\hat{\lambda}_{ds}^{s}}\right). \tag{5}$$

The generated electromagnetic torque of an IM is derived as

$$T_e = \frac{3P}{4}(\hat{\lambda}_{ds}^{s} i_{qs}^{s} - \lambda_{qs}^{s} i_{ds}^{s}), \tag{6}$$

where P is the IM pole number. The mechanical equation of the motor is obtained as

$$B_m\omega_{rm} + J_m p\omega_{rm} + T_L = T_e, \tag{7}$$

where B_m and J_m are the viscous friction coefficient and motor inertia, respectively, T_L is the load torque, and $\omega_{rm} = (2/P)\omega_r$ is the mechanical speed of the motor rotor shaft.

2.1 ST pattern and VSVPWM pattern closed-loop DTC IM drives

The ST pattern and VSVPWM pattern closed-loop DTC IM drives are shown in Figs. 1 and 2, respectively. Upon comparing Figs.1 and 2, it can be observed that the three-level torque hysteresis, two-level flux hysteresis, and voltage vector ST are replaced by the torque controller, flux controller, and VSVPWM, respectively.

The reversible transient and steady-state responses of the closed-loop DTC IM drive with a load of 2 N-m are shown in Fig. 3, including (a) rotor speed (ST pattern), (b) rotor speed (VSVPWM pattern), (c) torque (ST pattern), and (d) torque (VSVPWM pattern). Here, the speed and torque ripples of the VSVPWM pattern are less pronounced than those of the ST pattern.

The total harmonic distortion (THD, %) of the closed-loop DTC IM drive is shown in Fig. 4. The THD % for the ST pattern is 111.64%, whereas that for the VSVPWM pattern, is 41.05%. It is evident that the THD % of the VSVPWM pattern in the closed-loop DTC IM drive is lower than that of the ST pattern.

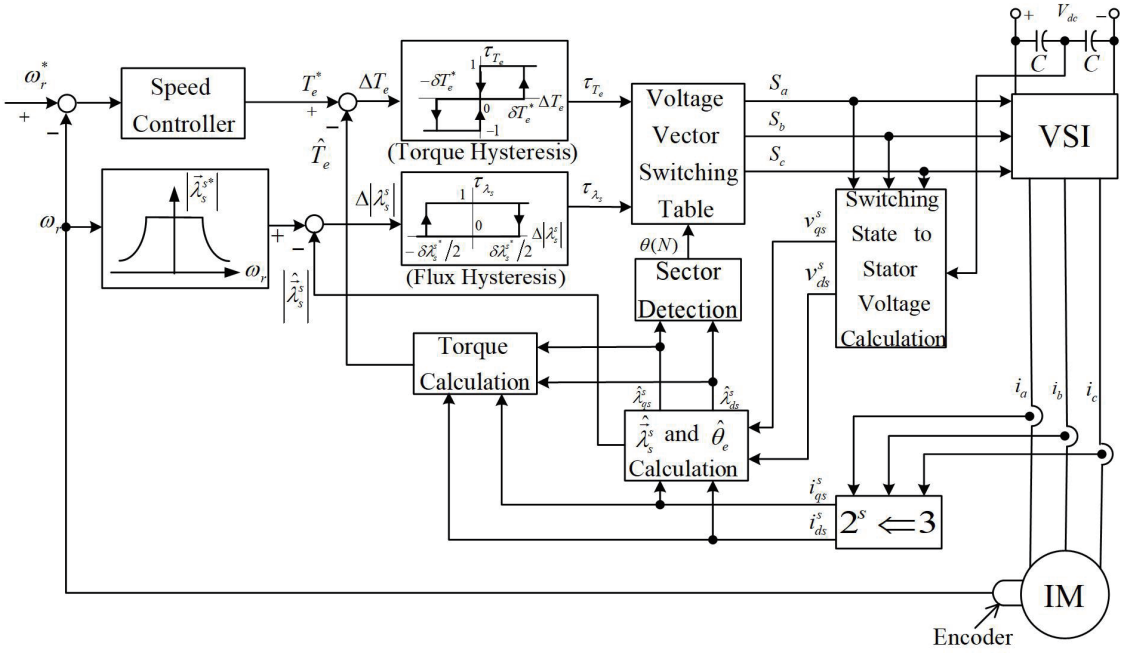

Fig. 1. ST pattern closed-loop DTC IM drive.

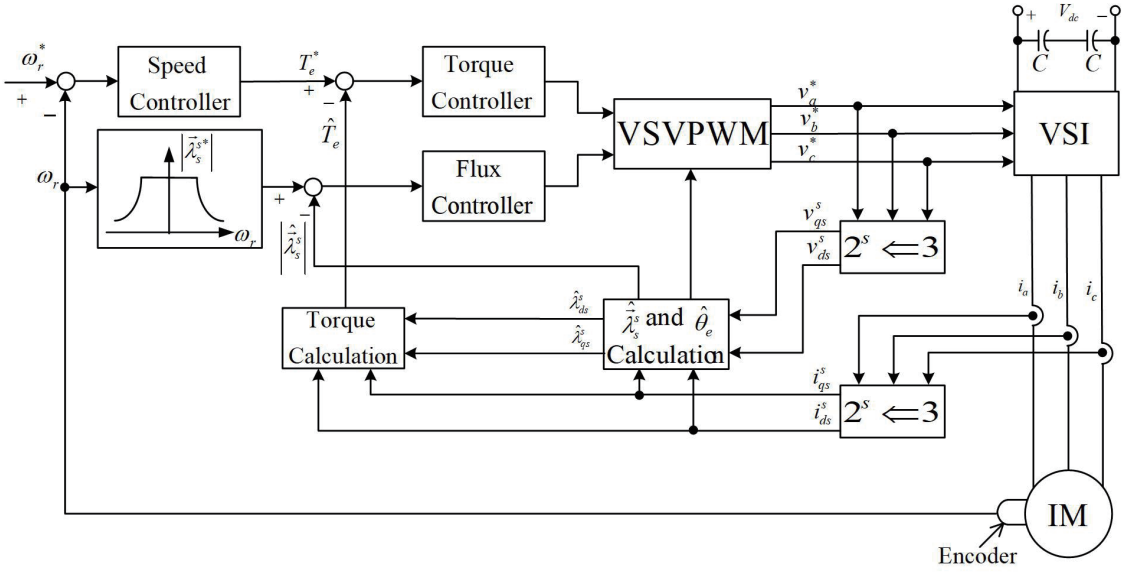

Fig. 2. VSVPWM pattern closed-loop DTC IM drive.

2.2 Rotor speed prediction using electromagnetic torque and rotor flux

The estimated rotor flux and the estimated synchronous speed can be respectively derived as

$$\hat{\vec{\lambda}}_r^s = \frac{L_r}{L_m}(\vec{\lambda}_s^s - \sigma L_s \vec{i}_s^s), \tag{8}$$

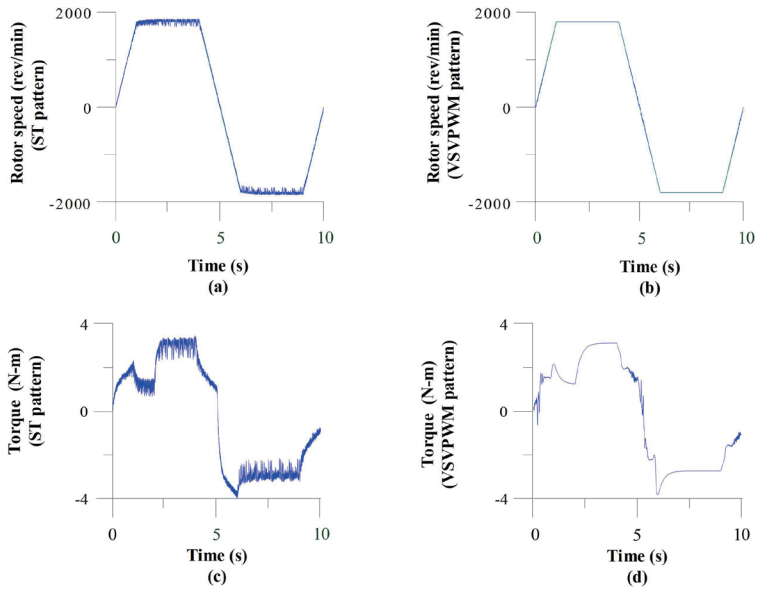

Fig. 3. (Color online) Speed and torque responses of the closed-loop DTC IM drive with a load of 2 N-m. (a) rotor speed (ST pattern), (b) rotor speed (VSVPWM pattern), (c) torque (ST pattern), and (d) torque (VSVPWM pattern).

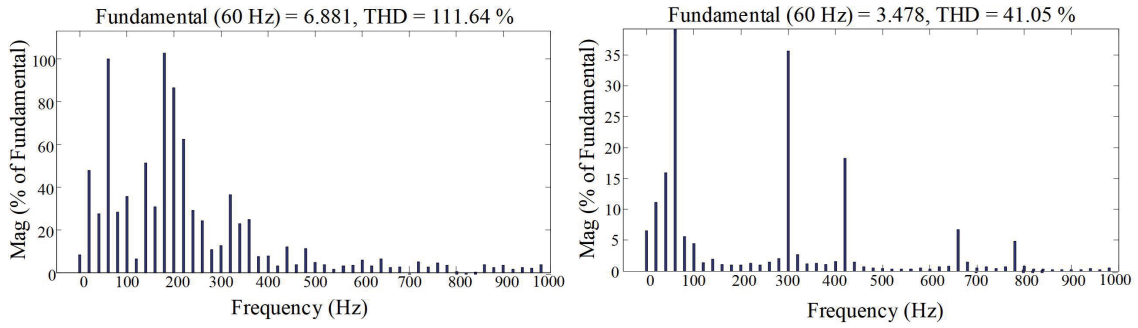

Fig. 4. (Color online) THD % of closed-loop DTC IM drive. (a) ST pattern and (b) VSVPWM pattern.

$$\hat{\omega}_e = \frac{\hat{\lambda}^s_{dr} s\lambda^s_{qr} - \lambda^s_{qr} s\lambda^s_{dr}}{\hat{\lambda}^{s\,2}_{dr} + \lambda^{s\,2}_{qr}}, \tag{9}$$

where L_s, L_r, and L_m are the stator, rotor, and mutual inductances, respectively, and $\sigma = 1 - L_m{}^2/L_sL_m$ is a leakage inductance coefficient.

The T-I-type equivalent circuit of an IM is shown in Fig. 5; here, s_{slip} denotes the slip. On the basis of the air-gap power of an IM, utilizing the voltage $|V_{AB}|$ between terminals A and B, and the current $|i_{Te}|$ entering between terminals C and D, the estimated slip speed can be derived as

$$\hat{\omega}_{sl} = \frac{4\hat{R}_r}{3P} \cdot \frac{\hat{T}_e}{\left|\hat{\bar{\lambda}}^{s2}_r\right|}. \tag{10}$$

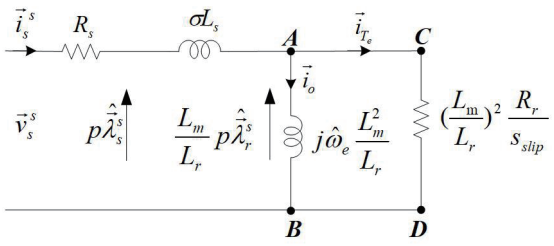

Fig. 5. T-I-type equivalent circuit of an IM.

The estimated rotor speed is obtained as

$$\hat{\omega}_r = \omega_e - \omega_{sl}. \tag{11}$$

3. MRAS Stator Resistance Parameter Identification Based on Active Power

The implementation of the speed prediction DTC IM drive requires accurate motor resistance parameters to estimate stator flux and synchronous speed. However, owing to temperature changes, the actual resistances of the motor may deviate from the set values, leading to the deterioration of the speed prediction DTC IM drive.

The active power of an IM absorbed from the power source is given by

$$P_s = i_{ds}^s v_{ds}^s + i_{qs}^s v_{qs}^s. \tag{12}$$

By substituting Eq. (1) into Eq. (12), the active power can be derived as

$$P_{s\_R_s} = \hat{R}_s (i_{ds}^{s\,2} + i_{qs}^{s\,2}) + i_{ds}^s s\hat{\lambda}_{ds}^s + i_{qs}^s s\lambda_{qs}^s, \tag{13}$$

where $\hat{R}_s$ is the identified stator resistance.

On the basis of the MRAS theory,[21] Eq. (12) without the identified parameter $\hat{R}_s$ is selected as the reference model, whereas Eq. (13) containing $\hat{R}_s$ is selected as the adjustable model. The difference between the reference model and the adjustable model is tuned by an adaptation mechanism. Assuming that the temperature coefficient of the rotor resistance is the same as that of the stator resistance, the estimated rotor resistance parameter is given by

$$\hat{R}_r = R_s (R_{rn} / R_{sn}), \tag{14}$$

where R_{rn} and R_{sn} are the nominal values of the rotor and stator resistances, respectively.

The MRAS stator resistance parameter identification scheme is shown in Fig. 6. Here, the stator resistance is the only plant parameter to be tuned, whereas the remaining state variables are either identifiable or measureable. The proposed identification scheme is robust with regard to variations in other plant parameters.

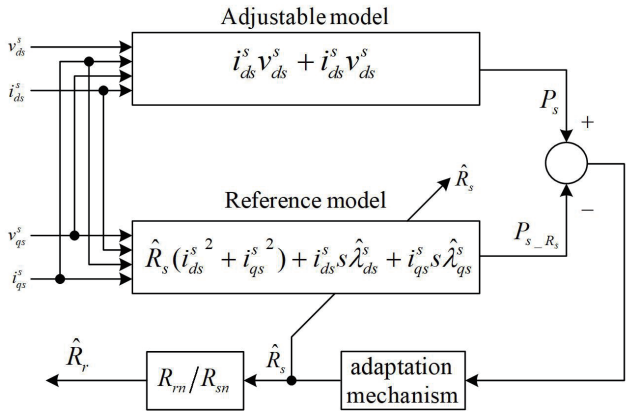

Fig. 6. MRAS stator resistance parameter identification scheme.

4. Adaptation Mechanism Design Using Modified PSO Algorithm

The modified PSO algorithm was employed to design the adaptation mechanism of the MRAS stator resistance parameter identification scheme. This choice was made owing to the advantages of having few setting parameters, fast convergence, and applicability to dynamic conditions. The PSO algorithm draws inspiration from the collective behavior observed in flocks of birds,[22] whereby individuals communicate special messages to steer the group towards a common goal. In PSO, each particle represents an individual within the group, equipped with memory and learning capabilities. Initially, a particle swarm is created with a uniform random distribution, with each particle serving as a candidate solution to the problem at hand. Through interactions guided by the best experiences of both individuals and the group, the particle swarm gradually approaches the optimal solution. However, the traditional PSO algorithm tends to converge rapidly towards local solutions. The inertia weight and maximum velocity methods improve the local solution convergence problem.[23] The process of updating particle positions and velocities is described as follows:

$$V_i(t) = w \cdot V_i(t-1) + C_1 \cdot Rand \cdot (P_{best} - x_i) + C_2 \cdot Rand \cdot (G_{best} - x_i), \tag{15}$$

$$x_i(t) = x_i(t-1) + V_i(t), \tag{16}$$

$$V_i(t) = \begin{cases} V_{max}, & \text{if } (V_i(t) \geq V_{max}) \\ V_{min}, & \text{if } (V_i(t) \leq V_{min}) \end{cases} \tag{17}$$

where $V_i(t)$ and $x_i(t)$ are the velocity and position of the particle, P_{best} and G_{best} denote the best solution positions for individual and group particles, respectively, C_1 and C_2 are the learning factors, w is a weighting, *Rand* is a random uniform distribution, V_{max} denotes the maximum velocity of the particle, and V_{min} is the minimum velocity of the particle.

Figure 7 shows the flow chart of the proposed modified PSO algorithm adaptation mechanism design.

Figure 8 illustrates the block diagram of the proposed speed prediction DTC IM drive incorporating motor resistance parameter identification. The system comprises a speed controller, a torque controller, a flux controller, VSVPWM, speed prediction based on $\hat{T}_e$ and $\hat{\lambda}_r^s$, $\hat{\lambda}_r^s$ and $\hat{\omega}_e$ calculation, $\hat{}_s^s$ and $\hat{\theta}_e$ calculation, torque calculation, three-phase to two-axis stationary

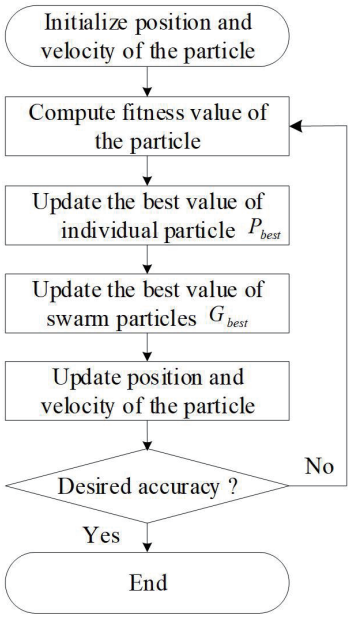

Fig. 7. Flow chart of the proposed modified PSO algorithm adaptation mechanism design.

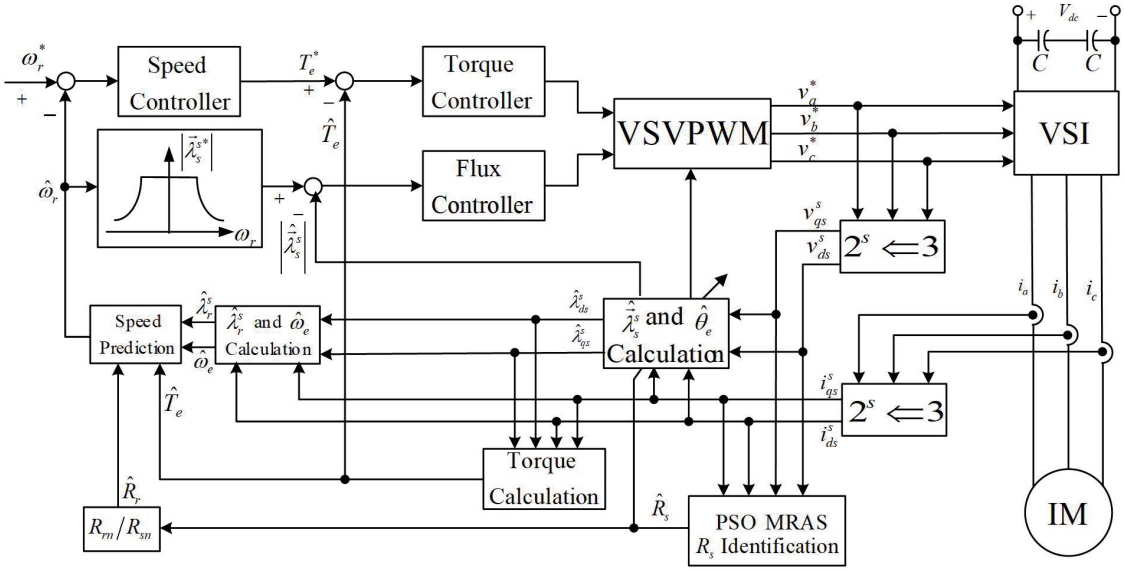

Fig. 8. Speed prediction DTC IM drive based on motor resistance parameter identification.

reference frame coordinate transformation ($2^s \Leftarrow 3$), and the PSO MRAS R_s identification scheme. In this system, the speed controller, torque controller, and flux controller were designed using the pole placement. The adaptation mechanism design was used in the modified PSO algorithm. Furthermore, the three-phase currents (i_{as}, i_{bs}, and i_{cs}) were obtained from the IM using Hall effect current sensors that achieved the coordinate transformation from a three-phase reference frame to a two-axis stationary reference frame ($2^s \Leftarrow 3$).

5. Simulation Setup and Results

A three-phase, 220 V, 0.75 kW, Δ-connected standard squirrel cage IM was used to serve as the controlled plant for experimentation to validate the effectiveness of the developed speed prediction DTC IM drive based on the MRAS stator resistance parameter identification. In a running cycle, the speed command is designed as follows: forward direction acceleration from $t = 0$ to $t = 1$ s, forward direction steady state running over $1 \leq t \leq 3$ s, forward direction braking to reach zero speed within the interval $3 \leq t \leq 4$ s, reverse direction acceleration from $t = 4$ to $t = 5$ s, reverse direction steady state running over $5 \leq t \leq 7$ s, and reverse direction braking to reach zero speed within the interval $7 \leq t \leq 8$ s. The simulated and measured responses of the first three running cycles are shown in Figs. 9 and 10, respectively. Here, the stator resistance was increased by 1 Ω at 9 s.

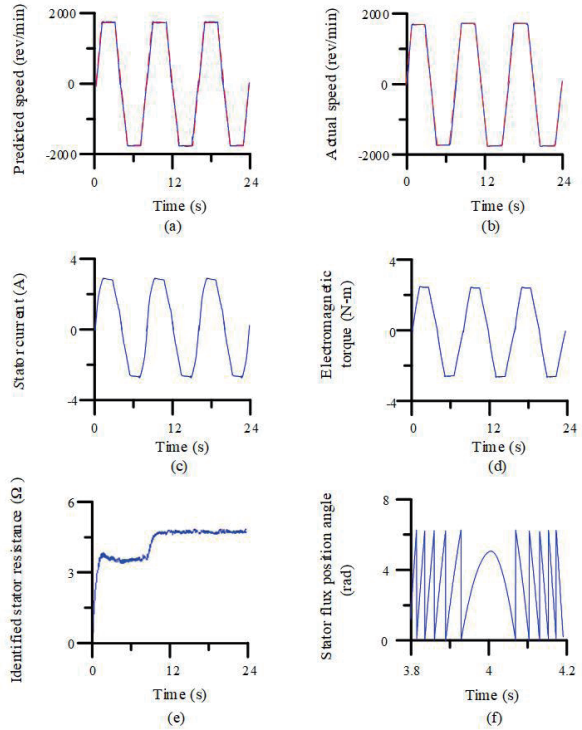

Fig. 9. (Color online) Simulated responses of the proposed speed prediction DTC IM drive based on the MRAS stator resistance parameter identification with a load of 3 N-m for a reversible steady-state speed command of 1800 rev/min: (a) predicted rotor speed, (b) actual rotor speed, (c) stator current, (d) electromagnetic torque, (e) identified stator resistance, and (f) stator flux position angle.

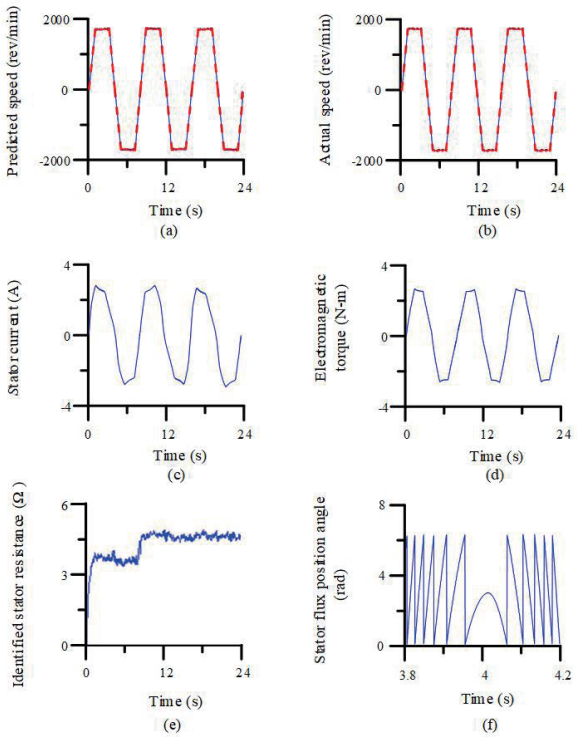

Fig. 10. (Color online) Measured responses of the proposed speed prediction DTC IM drive based on the MRAS stator resistance parameter identification with a load of 3 N-m for a reversible steady-state speed command of 1800 rev/min: (a) predicted rotor speed, (b) actual rotor speed, (c) stator current, (d) electromagnetic torque, (e) identified stator resistance, and (f) stator flux position angle.

Figures 9 and 10 present the simulated and measured responses with a load of 3 N-m for reversible steady-state speed commands at 1800 rev/min, respectively. Each figure contains six responses: (a) command (dashed line) and predicted (solid line) rotor speed, (b) command (dashed line) and actual (solid) rotor speed, (c) stator current, (d) electromagnetic torque, (e) identified stator resistance, and (f) estimated synchronous position angle.

According to the simulated and measured responses, the accurate determination of rotor speed was achieved through the integration of the electromagnetic torque and the estimated rotor flux. The MRAS stator resistance parameter identification scheme guarantees that speed prediction remains unaffected by resistance–temperature variations. Additionally, the sawtooth stator flux position angle ensurs the accurate determination of the synchronous speed. Promising responses were observed for electromagnetic torque and stator current, including reversible transient and steady states, indicating the effective realization of the desired performance. Consequently, the developed speed prediction DTC IM drive based on the MRAS stator resistance parameter identification scheme has shown that the desired performance can be achieved.

6. Conclusions

An MRAS stator resistance parameter identification scheme was developed for a speed prediction DTC IM drive. The DTC IM drive integrated with VSVPWM was established using the stator current and flux. The speed prediction was achieved through the utilization of electromagnetic torque and rotor flux. The MRAS stator resistance parameter identification was developed on the basis of the motor's active power, and the adaptation mechanism design was used in the modified PSO algorithm. The three-phase stator currents for implementing the speed prediction DTC IM drive were provided using the Hall effect current sensors. Simulation and experimental results under a load condition for reversible steady-state speed commands confirmed the promising performance of the proposed speed prediction DTC IM drive based on the MRAS stator resistance parameter identification scheme.

References

1 Y.-C. Luo, X.-H. Zheng, C.-H. Liao, and Y.-P. Kuo: Sens. Mater. **32** (2020) 1955. https://doi.org/10.18494/SAM.2020.2785
2 A. Devanshu, M. Singh, and N. Kumar: IEEE Trans. Power Electron. **35** (2020) 652. https://doi.org/10.1109/TPEL.2019.2912265
3 S. Shukla and B. Singh: IEEE Trans. Power Electron. **34** (2019) 5400. https://doi.org/10.1109/TPEL.2018.2868509
4 M. A. Khoshhava, H. A. Zarchi, and G. A. Markadeh: IEEE Trans. Energy Convers. **36** (2021) 3231. https://doi.org/10.1109/TEC.2021.3077829
5 G.-M. Sung, P.-Y. Chiang, and Y.-Y. Tsai: Proc. 2021 IEEE Int. Future Energy Electronics Conf. (IFEEC, 2021) 1–5. https://doi.org/10.1109/IFEEC53238.2021.9661986
6 S. Pradhan, S. Pani, and D. Puhan: Proc. 2022 2nd Odisha Int. Electrical Power Engineering, Communication and Computing Technology Conf. (ODICON, 2022) 1–5. https://doi.org/10.1109/ODICON54453.2022.10010289
7 S. Jnayah and A. Khedher: Proc. 2020 17th Int. Systems, Signals & Devices Conf. (SSD, 2020) 709–714. https://doi.org/10.1109/SSD49366.2020.9364128
8 I. M. Alsofyani and N. R. N. Idris: IEEE Trans. Power Electron. **31** (2016) 3027. https://doi.org/10.1109/TPEL.2015.2447731
9 R. Inan and R. Demir: Proc. 2019 1st Int. Global Power, Energy and Communication Conf. (GPECOM, 2019) 1–5. https://doi.org/10.1109/GPECOM.2019.8778459
10 Y. Azzoug, A. Menacer, R. Pusca, R. Romary, T. Ameid, and A. Ammar: Proc. 2018 Int. Applied and Theoretical Electricity Conf. (ICATE, 2018) 1–6. https://doi.org/10.1109/ICATE.2018.8551478
11 J. Chen and J. Huang: IEEE Trans. Power Electron. **33** (2018) 8695. https://doi.org/10.1109/TPEL.2017.2785330
12 X. Qi, W. Cao, and L. Aarniovuori: IEEE Trans. Ind. Electron. **70** (2022) 4516. https://doi.org/10.1109/TIE.2022.3189103
13 O. Lipcak, J. Bauer, and M. Chomat: Proc. 2019 Int. Electrical Drives & Power Electronics Conf. (EDPE, 2019) 255–260. https://doi.org/10.1109/EDPE.2019.8883887
14 J. Chen, J. Huang, and Y. Sun: IEEE Trans. Ind. Electron. **66** (2018) 2659. https://doi.org/10.1109/TIE.2018.2849964
15 M. Stender, O. Wallscheid, and J. Böcker: IEEE Trans. Power Electron. **36** (2021) 13261. https://doi.org/10.1109/TPEL.2021.3080129
16 G. B. Reddy, G. Poddar, and B. P. Muni: IEEE Trans. Ind. Appl. **58** (2022) 1416. https://doi.org/10.1109/TIA.2022.3141700
17 P. R. Savitha and B. P. Divakar: Proc. 2023 IEEE Int. Distributed Computing, VLSI, Electrical Circuits and Robotics Conf. (DISCOVER, 2023) 127–133. https://doi.org/10.1109/DISCOVER58830.2023.10316660
18 A. Nurettin and N. İnanç: IEEE J. Emerging Sel. Top. Power Electron. **11** (2023) 4332. https://doi.org/10.1109/JESTPE.2023.3265352

19 E. Zerdali, R. Yildiz, R. Inan, R. Demir, and M. Barut: Proc. 2018 XIII Int. Electrical Machines Conf. (ICEM 2018) 1367–1373. https://doi.org/10.1109/ICELMACH.2018.8507168
20 C. H. Liu: Control of AC Electrical Machines (Tunghua, Taipei, 2008) 4th ed., Chap. 6 (in Chinese).
21 Y.-C. Luo and Z.-S. Ke: Smart Sci. **6** (2018) 363. https://doi.org/10.1080/23080477.2018.1451207
22 A. Sahu, K. B. Mohanty, and R. N. Mishra: Proc. 2021 1st Int. Power Electronics and Energy Conf. (ICPEE, 2021) 1–6. https://doi.org/10.1109/ICPEE50452.2021.9358559
23 L. Yiyang, J. Xi, B. Hongfei, W. Zhining, and S. Liangliang: IEEE Access **9** (2021) 32341. https://doi.org/10.1109/ACCESS.2021.3059714